Research Square

Preprints are preliminary reports that have not undergone peer review.
They should not be considered conclusive, used to inform clinical practice,
or referenced by the media as validated information.

In Silico Insights of Tunable Small Molecules With Regulatory Activity of Acid Sphingomyelinase-Protein Kinase Cδ Interaction

Yellamandayya Vadlamudi
Pondicherry University
Kannan M
National University of Singapore
Thirunavukkarasu C
Pondicherry University
Suresh Kumar Muthuvel (suresh@bicpu.edu.in)
Pondicherry University https://orcid.org/0000-0001-7083-6565

Research Article

Keywords: acid sphingomyelinase, protein kinase C δ, protein-protein interactions, translocation, allosteric inhibition, Alzheimer's disease

Posted Date: October 26th, 2021

DOI: https://doi.org/10.21203/rs.3.rs-880986/v1

License: This work is licensed under a Creative Commons Attribution 4.0 International License.
Read Full License

Abstract

Acid sphingomyelinase demonstrates a housekeeping role and plays a key role in maintaining membrane turnover through sphingolipid metabolism. While deficiency of ASM housekeeping function leading to a lysosomal storage disorder, activation and translocation of ASM leads to AD pathology. Phosphorylation of ASM by PKCδ is critical for translocation of ASM to the plasma membrane. However, several strategies have been developed for the treatment of patients with AD, limitations of treatments and occurrence of AD by alternative signaling pathways become hurdle to the mortality of patients. In the present study, we report the interface of ASM- PKCδ interactions by performing molecular modeling, docking and dynamics simulation analysis. By considering the interacting site of ASM with PKCδ as an allosteric site, we screened a large number of small molecules by virtual screening and identified four lead molecules that show high binding affinity and interacting mode with residues of ASM that are critical to making interaction with PKCδ. The proven role of ASM in apoptosis, neurodegenerative diseases, and the existing functionality of leads in these diseases, together with strengthens the lead compounds, ZINC85551993, ZINC71928291, ZINC71773625 and ZINC85432419 as allosteric inhibitors for ASM. We believe that the lead molecules could be potential allosteric modulators for the translocation of ASM.

Introduction

A balanced Sphingolipid metabolism is essential to accomplish numerous cellular processes for the maintenance of normal physiological conditions. However, dysregulation of sphingolipid cues leads to numerous diseases including neurodegenerative complications. Alzheimer's disease (AD) is the most widespread dementia, accounting for up to 80% of dementia cases and it is more prevalence in aging population [1] [2]. AD is characterized by the accumulation of misfolded proteins, including amyloid β, thereby neurofibrillary tangles [3] [4]. While post-mortem evaluation is the definitive diagnosis of AD, recent research advances the diagnosis of AD in living patients by the detection of positron emission tomography (PET) and cerebrospinal fluid (CSF) biomarkers [5]. Additionally, more recently, several approaches have been established for diagnosis of AD, including non-invasive imaging to detect amyloid-β, evaluation of hyperphosphorylated tae peptide (p-tae), assay for circulating proteins of serum, and serum microRNA profiling [6] [7] [8] [9]. Along with establishment of diagnosis, researchers have been developed therapeutic approaches for the treatment of patients with AD. Cholinesterase inhibitors, including galantamine, donepezil and rivastigmine are currently recommended for the treatment of patients with mild-to-severe AD [10]. Memantine, an antagonist of N-methyl-D-aspartate receptor and agonist of dopamine is approved for the treatment of patients with AD [11]. In addition, huperzine A, omega fatty acid supplementation are also received attention in the implementation of AD treatment strategies [12] [13] [14].

Various lipid classes are much abundant in the cell membrane composition, and along with protein/receptors of cell membrane, these lipids demonstrate numerous cell signaling events to coordinate cellular organelles and cell environment [15]. Perturbation of membrane lipids leads to adverse effects and is the major underlie cause of AD pathology. Ceramide, a class of lipid has received

greater attention among the lipid classes as it contributes to AD pathology by affecting amyloid-β generation and phosphorylation [16] [17]. Emerging evidence has revealed that the lowering ceramide levels could reduce accumulation of amyloid-β, and indicated the importance of ceramide in therapeutic effectiveness [18] [19]. As a central signaling molecule in sphingolipid metabolism, ceramide can be produced by degradation of sphingomyelin, or synthesized *de novo* from sphingosine and fatty acyl coA [20] [21] [22]. Existing evidence has reported that acid sphingomyelinase (ASM) that involved in sphingomyelin hydrolysis, and acid ceramidase that responsible for ceramide synthesis, are expressed at elevated levels in AD [16] [23]. ASM, localized to lysosomes with an optimal pH, is play key role in ceramide formation by degradation sphingomyelin [24]. Moreover, an increased ceramide formation in lipid raft microdomins by the induction of activation and translocation of ASM has been identified [25]. Protein kinases are well-known to their indispensable role in activating substrate proteins. Accumulating evidence has revealed that protein kinase C delta (PKCδ) activates and translocate to plasma membrane by phosphorylation [26]. While the overexpression of PKCδ associated with neuronal damage, its inhibition results in reduction of cellular injury has been reported [27] [28] [29].

Although, several approaches has been developed in recent years to treat patients with AD, inefficacy of disease modifying and limitations of treatment, are still hurdle in mortality of patients with AD [30]. Moreover, identifying the potential signaling pathways in AD pathology is being increased for the implementation of AD clinical settings. Based on the facts, we believe that ASM-PKCδ signaling is a major contribution to AD pathology. In this study, we explore ASM-PKCδ binding interface by molecular docking and molecular dynamics simulation. We further screened a large number of small molecules against PKCδ binding site of ASM to identify lead molecules as the allosteric inhibitors.

Materials And Methods

Full-length Structure prediction of PKCδ and ASM

In order to understand the molecular interaction between PKCδ and ASM, the full length model of PKCδ was predicted by using Robetta server [31] [32] that demonstrates homology modeling and ab initio methods. The sequence of PKCδ (UniProt ID: F1MZX0, 676aa) was retrieved from the UniProt database (http://www.uniprot.org) and subsequently performed protein BLAST against the Protein Data Bank (PDB, http://www.rscb.org/pdb/) to identify homologue templates. Due to lack of homologous template, Robetta server was used to model the protein structure. Robetta server aligns PKCδ sequence with extended-synaptotagmin (PDB ID 4P42), protein kinase C γ (PDB ID 2E73), human chymerin1 (PDB ID 3CXL), lambda cro (PDB ID 3A63) and protein kinase alpha (PDB ID 3IW4). Based on the essentiality of zinc metal ion for its activity, the obtained model was remodeled using Modeler9v8 program [33] to fix four zinc metal ions. As a final step of structure prediction, the least Modeler Objective Function (MOF) and Discrete Optimized Protein Energy (DOPE) [34] score were considered to select the best model selection. Further, the model was validated by the Structural Analysis and Verification Server (SAVES) server that contains PROCHECK and ERRAT [35].

The full length ASM structure prediction was clearly described in our previous study [36]. However, recently the crystal structure of human acid sphingomyelinase (PDB ID 5JG8) with unsolved small portions of N-terminal and C-terminal regions was deposited in the protein data bank [37]. Thus, the crystal structure was taken into consideration as a template to remodel our previous ASM model using Modeler9v8 program. The aforementioned procedure was followed for the selection of the best model, and subsequent structural verification.

Structural preparation of PKCδ

To attain active state of PKCδ, docking was performed with ATP molecule at the region of ATP binding site; ATP (CID: 5957) was downloaded from PubChem database (http://pubchem.ncbi.nlm.nih.gov/search/search.cgi) and followed ligand preparation using LigPrep module of Maestro (Schrödinger 2014-2) software by assigning OPLS-2005 force field. At this point, the most occurring possible ionization states at pH7.0 ± 2.0 were set up with their specified chiralities. The PKCδ protein was prepared to adapt the bond order and setting the hydrogens using the protein preparation wizard, which is embedded in Maestro. Further, hydrogen bonds were assigned based on the sample water orientation, and optimized by exhaustive sampling methods. Moreover, the protein was subjected to energy minimization by applying OPLS 2005 force field. Residues (355–363) of PKCδ, those proven as ATP interacting residues were selected to generate receptor grids. The grid of about 10 Å radius was created to dock the molecule by following the standard precision (SP) protocol of Maestro.

Molecular dynamics simulation of PKCδ and ASM

To check the structural stability, MD simulation of PKCδ and ASM was performed using GROMACS 5.1.0 molecular dynamics package [38] [39]. The topology information of ATP molecule was generated based on PRODRG Server and the topology files of PKCδ and ASM were generated using pdb2gmx command. GROMOS96 54a7 force field was used to assign the proper bond order and geometrical parameters of the proteins. Moreover, the systems with cubic box (distance of 1.0 nm from the center of the protein to edge of the box) were solvated using SPC216 water model, and periodic boundary conditions were applied to maintain the directions of systems. Based on the net charge of systems, water molecules were replaced with Cl- ad Na + counter ions. Next, energy minimization of proteins was performed using steepest descent algorithm with a tolerance of $1000 kJmol^{-1}nm^{-1}$. Moreover, interactions including electrostatic and Van der Waals were applied by using Fast particle-Mesh Ewald electrostatics (PME) [40] with 1nm cut off. LINCS and SETTLE algorithm were used to constrain the bond angles and geometry of the water molecules, respectively. While, Parrinello-Rahman [41] method was used regulate the pressure, the modified weak coupling berendsen thermostat and V-rescale algorithm were used to regulate the temperature of the systems. The distance restraints method (the distance ranging between 2.3 and 3.3 Å) was used to retain the coordination bonds formed between Zn2 + metals and metal binding residues. The residues including D202, H204, D274, N314, H421, H453 and H455 of ASM, and C189, C208, C192, H159, C172, C200, C175, C280, C264, C261, H231, C244, C247 and C272 of PKCδ were involved in the formation of coordination bonds. Both NVT (constant number of particles, volume and temperature) and NPT

(constant number of particles, pressure and temperature) were accomplished for 100 ps, and checked for their equilibration status. After equilibration, MD run for about 50ns of production was performed with a time frame of 2 fs. The dynamics and structural transitions of PKCδ and ASM were analyzed using the tool of GROMACS package.

The PCA and FEL analysis

The high amplitude concerted motions of protein in simulated trajectories through eigenvectors of the covariance matrix were determined by using PCA and dPCA analysis [42]. Accordingly, the PCA of PKCδ and ASM proteins were calculated to demonstrate the atomic motions of the proteins during the course of MD simulation. The cosine content (cj) was calculated for each principal component (pi) of covariance matrix to signify the free energy landscape [43] [44]. These sensitive measures of trajectories enable mapping free energy landscape of chosen principal components (PCs), which describes further conformational changes of proteins. In general, the values of cosine content ranging between 0 (no cosine) and 1 (perfect cosine) in the total time of simulation period (T):

While, the structural dynamics of protein can be understand by the first eigenvector cosine contribution, in most of the cases, the value of the first eigenvectors cosine shows closer to 1. As the high cosine content represents the large-scale motions, the first cosine content, generally, is not suitable for analyzing FEL. However, recent studies reported that the cosine contents possess the value ranging below 0.2 or sometime up to 0.5 can result accurate conformational mapping [44]. Therefore, here, the first 20 PCs of each protein were analyzed based on their cosine values. FEL was prepared using cosine contents, which showed lesser than 0.2 of the first two projection eigenvectors and were represented as PC1 and PC2 respectively. These analyses provided the energy minima of each protein, which further led to point out the best free energy conformation of PKCδ and ASM.

Protein-Protein interaction studies

To understand the structural interacting pattern of ASM, protein-protein docking was performed between PKCδ with ASM using the High Ambiguity Driven Bio-molecular Docking (HADDOCK) [45] [46]. The most stable conformations of both ASM and PKCδ with lowest free energy were prepared by assigning the hydrogen atoms followed by minimization. PKCδ interacting region of ASM from literature was used as active site residues for docking purpose, while the neighboring amino acids of the active site were taken as passive residues. The best cluster was selected based on the HADDOCK score and RMSD cut-off of 7.5 Å, and further analysis was performed by using PISA (Protein Interfaces, Surfaces and Assemblies) web interface. A binding free energy of docked complex was calculated using PDBePISA interface [47] [48]. Moreover, molecular dynamics simulation of ASM-PKCδ complex was performed to understand the structural transitions of ASM upon interaction with PKCδ.

Free energy calculations

Molecular mechanics Poisson Boltzmann or Generalized Born solvent accessible surface area [MMPB (GB) SA] [49] [50] is a computational tool used for the analysis of bio molecular interactions. The principles behind this method are well authorized and used effectively in earlier studies [49]. In recent years, several drug discovery studies have used this tool as a scoring function. Here, the free energy of protein-protein complex was obtained by using MMPBSA algorithm through Gromacs 5.1.0. The equilibration region (50–80 ns) trajectory was used for this application. All water molecules and ions were removed from the trajectory. The free energy calculations were determined by the following equation:

ΔG binding= $\{G^{complex}(i)\} - \{G^{protein1}(i)\} - \{G^{protein2}(i)\}$

Molecular interactions of ASM allosteric site

To identify allosterically binding lead compounds, lowest energy conformation of ASM was selected through MDS and PCA analysis. Accordingly, the protein was prepared in multistep process using protein preparation wizard of Schrodinger software. After adding hydrogen and bond order assignment, the protein was subjected to energy minimization by OPLS2005 force field. The grid was generated by using allosteric site information from ASM-PKCδ docking and experimental evidence. A total of 958771 library of compounds from zinc data base were retrieved and prepared via ligprep module in Schrodinger software. The prepared ligand compounds were docked into ASM allosteric site through High Throughput Virtual Screening (HTVS) using glide maestro module. The successful 10% compounds of HTVS were taken up to SP docking for further screening. Finally, to eliminate false positive results, the best 10% compounds from SP docking were allowed for XP docking. The results obtained in virtual screening were analyzed. The figures were prepared using glide maestro module of Schrodinger and chimera software.

Results And Discussion

Structural analysis of PKCδ

The modeled full length PKCδ protein indicates that the structure is composed of regulatory (1-329) and catalytic (330–676) subunits. The regulatory subunit consists of three small domains include a C2 domain (1-146) which is believed to be non-calcium binding domain and two Zinc finger motifs (158–208 and 230–280). The C2 domain comprises of 8 β strands that are involved in the formation of β sheet, and one helix. The catalytic subunit is composed of a protein kinase domain (349–603) and an AGC-kinase C-terminal domain (604–676) (Fig. 1). The protein kinase domain is composed of N-lobe and C-lobe and these two lobes are joined by a hinge linker region. This type of arrangement of protein kinase domain of bovine PKCδ shows homologue nature with other protein kinases. Six-stranded β-sheet and three α-helices collectively forms the N-lobe whereas the C-lobe consists mostly of helical structural elements (8 helices) and two β-strands. The ATP molecule binds in the ATP binding region (355–363) through hydrogen bond formation. Consequently, the β phosphate oxygen atom O8 forms hydrogen bonds with K378 and A490 with contact distance of 2.92 Å, 2.44 Å whereas the O5 oxygen atom forms

hydrogen bonds with K378 with a contact distance of 3.04 Å respectively. The O2 and O3 atoms of the ribose moiety forms two non-classical hydrogen bonds with the backbone oxygen atom of N478 with a distance of 2.96 Å and 2.64 Å respectively. The NH2 atom of purine ring forms classical hydrogen bond with D634 oxygen atom of PKCδ with a distance of 3.03 Å. In addition, F633 (CZ) forms T-shaped π-π interaction with Cg of purine and pyrimidine moiety with contact distance of 4.1 Å and 3.8 Å respectively. The residues L401, F360, L480, V363, A376, A490, F637 and M427 forms hydrophobic interactions whereas T411, N478, K475, E397 and D477 forms polar and charged interactions with ATP (Fig. 2). All these interaction analysis shows that ATP resides in perfect binding mode at the ATP binding cavity as like in other PKC kinase family proteins with the Glide energy of -56.975 kcal/mol.

Structural analysis of ASM

The full length ASM model details were described in our previous publication [36]. However, after remodeling based on recently available human ASM crystal structure, the ASM structure has adapted some additional features. The full length ASM is comprised of three different domains, which includes N-terminal domain (NTD), phosphoesterase domain (PED) and C- terminal domain (CTD). The helical domains (contains only helices) NTD and CTD are positioned at the angle and distance of 45.6˚ and 23 Å with respect to the domain axis. The PED domain is placed with angle and distance of 83.2˚ and 7.8 Å from NTD and 50.0˚ and 16 Å from CTD (Fig. 3). The N-terminal domain comprises a total of 6 helices. The helices α1 (C29-A42) and α2 (K66-L74) were placed parallel to each other. The helices α3 (T84-L99), α4 (Q102-L119), α5 (P124-T143) and α6 (a152-L156) contributes to the formation of saposin B type domain and plays a role in lipid binding. Unlike, previous ASM model, saposin B type domain of remodeled ASM adopted open confirmation and this domain has moved towards the catalytic cavity. This clearly indicates that after lipid binding, saposin B type domain handover the lipid molecule to the catalytic site for its hydrolysis. The PED contains totally 9 helices (α 7- α 15) and 9 beta strands (β 1- β 9). Among 9 β strands, β4, β5, β6 and β7 have contributed to the catalytic site and oriented in such a way that the residues H421, H453 and H455 have coordinate interactions with zinc metal ions along with H203, D202, D274 and N314 residues. Particularly, the long loop region (D206-L248) has adopted open conformation by giving a way for the substrate entry into catalytic cavity. This confirmation is similar to ASM structure at pH 5.0 of our previous study.

Molecular dynamics simulation

To understand the structural stability of PKCδ and ASM, protein structures were subjected to molecular dynamics simulation studies at 50 ns for each protein. The backbone RMSD of PKCδ has shown higher fluctuations (0.5-1.75nm) upto 25 ns and then it was well equilibrated till 50 ns MD run. The backbone RMSD profile clearly indicates that PKCδ protein attains stable conformation from 25-50ns production MD run with little RMSD fluctuations (Fig. 4A). Further, the RMS fluctuation data of PKCδ indicates that more number of residues (125–150) of the C2 domain have higher fluctuations upto 1.8 nm whereas in other domain (zinc finger domains and protein kinase domain) only few residues have shown higher fluctuations.(Fig. 4B). The same analysis was carried out for ASM to know the protein stability by means of RMSD fluctuations. The RMSD profile of ASM shows that the protein took first 15 ns time period to

reach equilibration state and subsequently equilibrated till 50 ns MD run with very less RMSD fluctuations. This clearly depicts that ASM is energetically stable for about 35 ns time scale of MD run (Fig. 4A). The RMS fluctuation profile shows that maximum number of residues of the signal peptide has higher fluctuations up to 1.25 nm. Residues of saposin B type domain have fluctuation up to 0.5 nm, and the residues of other domains like PED and CTD have very less fluctuations compared to NTD (Fig. 4C). This analysis clearly depicts the overall stability of individual domains of PKCδ and ASM.

Structural transitions of PKCδ

In order to understand the structural transitions attained in the MD run production, representative structures were extracted and explored based on the Principle Component Analysis and Free Energy Landscape graph. Accordingly, the first two principle components that show less than 0.2 cosine content were used to construct the FEL graphs. The contour map of the FEL analysis showed three different minimum energy clusters (Fig. 5). Representative structure of cluster 1 indicates that the C2 domain (C2D) is placed at about 27.1 Å distance from the Zinc finger domain (ZFD) whereas representative structures of cluster 2 and 3 moved closer with distance of 21.0 and 23.5 Å respectively, based on the domain-domain distance analysis (Table 1). The ZFD and Catalytic domain (CD) distance in cluster 1, 2 and 3 were about 27.4, 28.3 and 27.4 Å respectively, which clearly shows the compact nature of ZFD with CD throughout the time period of production MD run. In cluster1 and 2 the catalytic domain is placed at about 39.9 and 36.8 Å distance respectively with C2D whereas in cluster3 the C2D moved away from the catalytic domain with a distance and angle of 43.7 Å and 18.9˚ respectively. The AGC kinase domain loses its secondary structural elements in the cluster2 representative structure. Thus, Based on the domain distance analysis of clusters, cluster 1 was found to be best for further docking studies.

Table 1
Domain-Domain movement comparison of FEL representative structures of PKCδ

Domain-Domain	FEL representative structure					
	Structure1		Structure2		Structure3	
	Angle(˚)	Distance(Å)	Angle(˚)	Distance(Å)	Angle(˚)	Distance(Å)
C2D-ZFD	16.6	27.1	28.0	21.0	8.0	23.5
ZFD-CD	27.3	27.4	8.2	28.3	12.0	27.4
C2D-CD	16.3	39.9	21.7	36.8	18.9	43.7

Structural transitions of ASM

In the case of ASM structure, FEL analysis showed two free energy minimum clusters based on the first two principle components. The representative structure of each free energy minimum cluster was extracted and displayed in Fig. 6. NTD maintained an average distance of 24.1Å from PED in both FEL

representative structures whereas CTD was placed at the distance of 20.2Å in average. There is no much deviation in the domain-domain movement of both representative structures. The loop region (206–248) which is believed to be controlling substrate entrance was displaced away from the catalytic cavity in both representative structures. Therefore, based on the free energy minimum cluster population, the cluster1 is selected as a best cluster and representative structure of this cluster used for protein-protein docking studies. Domain-Domain distances and angle of ASM structure were shown in Table 2.

Table 2
Domain-Domain movement comparison of FEL representative structures of ASM

Domain-Domain	FEL representative structure			
	Structure1		Structure2	
	Angle(˚)	Distance(Å)	Angle (˚)	Distance (Å)
NTD-PED	39.9	23.3	35.7	25.0
PED-CTD	49.4	20.9	43.3	19.5
NTD-CTD	13.9	41.9	9.5	42.5

Table 3

A) Solvation free energy of molecular complex calculated by using PDBePISA B) Hydrogen bonds formed between PKCδ and ASM and C) salt bridges formed between PKCδ and ASM. The distance of hydrogen bonds and salt bridges are in Angstrom

ID	Structure1			Structure2			Interface Area, Å2	ΔiG	NHB	NSB
	Mol	iNat	iNres	Mol	iNat	iNres		Kcal/mol		
Interfaces between PKCδ and ASM										
1	PKCδ	154	50	ASM	138	42	1369.5	-15.4	16	5
Hydrogen bonds										
S.No	Residues of PKCδ			Distance (Å)			Residues of ASM			
1	A:ARG 643[HH22]			1.81			B:SER 192[OG]			
2	A:CYS 509[HG]			1.77			B:GLN 407[OE1]			
3	A:GLY 356[N]			2.79			B:TYR 500[OH]			
4	A:ARG 643[HH11]			2.19			B:TYR 500[O]			
5	A:GLY 358[N]			3.26			B:SER 501[OG]			
6	A:LEU 644[N]			3.44			B:GLY 502[O]			
7	A:ARG 643[HH11]			1.83			B:SER 503[OG]			
8	A:SER 506[O]			3.82			B:ALA 176[N]			
9	A:ASP 383[OD2]			1.62			B:LYS 186[HZ3]			
10	A:ASP 477[OD2]			1.99			B:ARG 412[HE]			
11	A:ASN 478[OD1]			1.81			B:ARG 412[HH21]			
12	A:PHE 637[O]			1.78			B:TYR 500[HH]			
13	A:GLY 356[O]			3.06			B:SER 501[OG]			
14	A:SEP 645[O3P]			2.70			B:GLY 502[N]			
15	A:SEP 645[OG]			3.24			B:SER 503[N]			
16	A:SEP 645[O3P]			3.53			B:SER 503[N]			
Salt bridges										
1	A:ARG 643[NH2]			3.55			B:ASP 497[OD1]			
2	A:ASP 383[OD2]			2.61			B:LYS 186[NZ]			
3	A:ASP 477[OD2]			2.82			B:ARG 412[NE]			
4	A:ASP 477[OD1]			2.70			B:ARG 412[NH2]			

ID	Structure1			Structure2			Interface Area, Å2	ΔiG	NHB	NSB
	Mol	iNat	iNres	Mol	iNat	iNres		Kcal/mol		
5	A:ASP 477[OD2]			2.81			B:ARG 412[NH2]			

Molecular docking of PKCδ-ASM

Several studies have revealed that the interaction of PKCδ shows the influential effect on translocation of ASM from lysosomes to the plasma membrane. In order to understand the molecular level interacting mechanism, the selected representative structures of PKCδ and ASM were used for protein-protein docking. The PKCδ and ASM formed complex with an interface area of 1369.5Å2, constituted by 50 residues of PKCδ and 42 residues of ASM with − 15.4 kcal/mol solvation free energy gained upon interface formation. Both polar and non-polar residues collectively form 16 hydrogen bonds and 5 salt bridges with less hydrophobic contacts. The residues R643, C509, G356, G358, L644, S506, D383, D477, N478, F637 and S645 of PKCδ forms strong hydrogen bonds with the residues S192, Q407, Y500, S501, G502, S503, A176, K186 and R412 of ASM (Fig. 7). The residue S645 of PKCδ which is proven to be an auto phosphorylated residue formed a hydrogen bond with S503 residue of ASM by the contact distance of 3.2Å. This S503 residue is a neighboring residue of S504, which is the site for phosphorylation of ASM and thus these interactions are essential for making phosphorylation process possible.

Structural stability analysis of the bio molecular complex

To check stability of ASM upon complex formation with PKCδ, the complex structure was subjected to molecular dynamics simulation for about 80 ns MD run based on the earlier mentioned molecular dynamics simulation protocol. The backbone RMSD profile of complex was generated and analyzed. Initially, RMSD fluctuation was raised up to 1nm, and was continued up to 35 ns time scale (Fig. 8A). After 35 ns time scale, the RMS fluctuation restrained of about 0.2nm fluctuation range, which continued till 80 ns with a minimum RMSD fluctuation. Additionally, the hydrogen bond profile shows that 5–10 hydrogen bonds were well maintained in the equilibrated region of 50-80ns MD run describing the stable conformation of the complex (Fig. 8B). Moreover, the FEL analysis showed only one free energy minimum cluster based on the first two principle components. The representative structure from this free energy minimum cluster is extracted and displayed in Fig. 9, which indirectly claims that the transition of the complex was restricted as the stability is maintained upon complex formation. In addition, the interacting complex was subjected to MMPBSA calculation to find the binding free energy of protein-protein complex structure in the equilibrated region of MD simulation. Accordingly, best complex shown the binding energy of -585.613 +/- 222.974 $kJmol^{-1}$ (Table 4).

Table 4
The van der Waals, electrostatic, polar solvation, SASA and Binding energy calculated using MM-PBSA tool specifically designed for Gromacs MD package.

MM-PBSA complex	Van der Waals (kJ mol-1)	Electrostatic Energy (kJ mol-1)	Polar solvation Energy (kJ mol-1)	SASA energy (kJ mol-1)	Binding Energy (kJ mol-1)
PKCδ- bASM	-357.996 (+/- 25.922)	-839.070 (+/- 101.172)	651.592 (+/- 221.792)	-40.139 (+/- 9.696)	-585.613 (+/- 222.974)

Allosteric interacting lead molecules

Accumulated evidence has revealed that the deficiency of ASM in lysosomes leads to a rare lysosomal storage disorder, called Niemann-Pick disease[51] [52] [53] [54] [55], thus ASM functional activity is very essential. However, its translocation to plasma membrane and subsequent ceramide elevation leads to AD. Hence, we aim to identify inhibitor molecules that could restrict ASM translocation. As an allosteric site, ASM interface that interacts with PKCδ was docked with a library of ligands and the docking results were analyzed. Among the library of compounds, the top four hits were selected based on binding mode, XP score and glide emodel scores. Zinc database code of each ligand and their structures were displayed in Table 5.

Table 5: The best lead compounds for allosteric inhibition of ASM

ZINC85551993	ZINC71928291	ZINC85432419	ZINC71773625
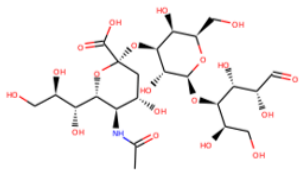	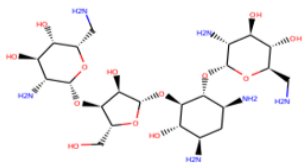	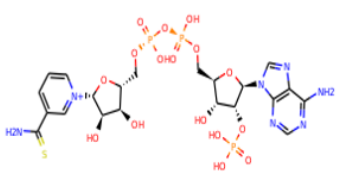	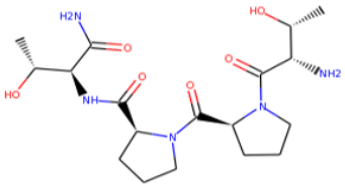

Among all the 4 selected complexes, the ligand of docking complex ASM-ZINC85551993 showed with better docking score of -10.292, and glide emodel energy of -78.569. Atom H33 of ligand positioned towards oxygen atom of S503 residue and formed hydrogen bond with distance of 1.96 Å, whereas oxygen atom of G413 residue showed two hydrogen bonds with H29 and H30 of ligand with bond distance of 1.95 and 1.92 Å respectively. At the same time atoms H36 and H37 of ligand showed hydrogen bonds (1.87 and 2.47 Å) with OG1 group of T445. Other atoms H25 and O13 of this ligand also form hydrogen bonds with E410 (1.71 Å) and N444 (1.95 Å) respectively. The complex formation of this ligand with ASM and interacting mode with hydrogen bonding and other interactions were displayed in

Fig. 10A. Interestingly, ZINC85551993 (3'-Sialyllactose) has patented for its apoptotic activity (PATENT CN-110123822-A). While the role of acid sphingomyelinase in membrane associated, ceramide-induced apoptosis signaling has been reported [56]. These observations of molecular docking of ZINC85551993 with ASM, its pro-apoptotic activity, and ASM role in apoptosis, are strengthen allosteric binding efficacy of ZINC85551993.

Interacting complex of ASM-ZINC71928291 showed that ligand molecule have hydrogen bonds with S501, S503, H505, E410, D414 and E443. The H36 of ligand faced towards oxygen atom of S503 and formed hydrogen bond with 2.08 Å. Hydrogen atoms 37, 35 and 31 of ligand shown hydrogen bonds with ND1 group of H505, OG group of S501 and oxygen atom of D414 with 2.28, 1.78 and 1.81Å respectively. To stabilize the complex further, H44 (1.80 Å) and H42 (1.99 Å) groups of ligand formed two hydrogen bonds with OE2 group of E410 residue. Additionally, OE2 group of E443 involved in the formation of two hydrogen bonds with H26 (2.25 Å) and H27 (1.89 Å). This complex has shown XP score of -9.468 with glide emodel energy of -90.133. Atoms and groups of ASM and ligand, which are participated in hydrogen bonding, were shown in Fig. 10B. A recent study has revealed that gentamycin, an antibiotic used for treatment of many anti-microbial infections, targets ASM in cancer cells [57]. This report gives a hope that ZINC71928291 (neomycin), a compound of antibiotic class binding at allosteric site of ASM could be potential lead molecule for the evaluation of its efficacy in AD.

The interaction of ZINC85432419 ligand with allosteric site of ASM was stabilized by 6 hydrogen bonds, and the ligand possesses docking score of -7.958 and glide emodel score of -67.997. The groups H22 and O11 of ligand establish hydrogen bonds with oxygen atom of S503 and hydrogen atom of G502 with distances of 1.74 and 2.14 Å respectively. Another hydrogen group H22 of ligand form hydrogen bond with OG group of S501with distance of 2.60 Å, whereas O5 and O14 atoms positioned towards HZ2 group of K415 and 2HD2group of N444 and formed hydrogen bonds with distances of 1.98 and 1.90 Å respectively. The complex also stabilized by constitutes hydrogen bond between H25 and Oxygen group of E410 with distance of 1.93 Å (Fig. 10C).

Formation of hydrogen bonds with S501, S503, G413, E443, T445 and N444 allows ZINC71773625 ligand to fit into the allosteric site giving a docking score of -7.625 and emodel score of -70.273. Atoms H27, H28 and H22 of ligand showed hydrogen bonding with oxygen of OG group of S501 and oxygen atom of G413 by the distance of 1.93, 2.19, 1.98 and 2.31 Å respectively (Fig. 11C). H30 atom of ligand with distance of 1.78 Å showed hydrogen bonds with OE2 group of E443. O1 atom of this ligand showed hydrogen bond with 1HD2 group of N444 by the distance of 2.37 Å (Fig. 10D). We recognized that ZINC71773625 (rapastinel) is a potent anti-depressant agent, and act as an allosteric modulator of N-methyl-D-aspartate receptor [58]. Based on our docking results and existing evidence, we believe that this lead molecule could also be a possible allosteric modulator of ASM. For the four complexes, the interacting residues were listed in the Table 6.

Table 6
Residues of ASM involved in the interactions with lead compounds

Molecules	Hydrogen-bonding interactions			Residues involved in polar and non polar interactions	Glide docking score	Glide emodel score
	H-bond donar	H-bond acceptor	Bond length (Å)			
ZINC85551993	Lig:H33	S503: O	1.96	H505, K415, R441, P180 and Y442	-10.292	-78.569
	Lig:H29	G413:O	1.95			
	Lig:H30	G413:O	1.92			
	N444:HD2	Lig:O17	1.95			
	Lig:H36	T445:OG1	1.87			
	Lig:H37	T445:OG1	2.47			
	Lig:H25	E410:OE2	1.71			
	Lig:H23	E443:OE2	1.84			
	Lig:H24	E443:OE2	1.86			
	N444:2HD2	Lig:O13	1.95			
	Q183:HE2	Lig:O6	2.00			
ZINC71928291	Lig:H37	H505:ND1	2.28	G502, G413, D411, Y442, Q183, P180, K415 and T445	-9.468	-90.133
	Lig:H31	D414:O	1.81			
	Lig:H35	S501:OG	1.78			
	Lig:H36	S503:O	2.08			
	Lig:H40	E410:O	2.12			
	Lig:H44	E410:OE2	1.80			
	Lig:H42	E410:OE2	1.99			
	Lig:H27	E443:OE2	1.89			
	Lig:H26	E443:OE2	2.25			

Molecules	Hydrogen-bonding interactions			Residues involved in polar and non polar interactions	Glide docking score	Glide emodel score
	H-bond donar	H-bond acceptor	Bond length (Å)			
ZINC85432419	G502:H	Lig:O11	2.18	E443, S504, K186, D414, T445, G413 and H505	-8.739	-67.997
	Lig:N4	Q184:HE2	2.12			
	Lig:H25	E410:O	1.93			
	K415:HZ2	Lig:O5	1.98			
	N444:2HD2	Lig:O6	1.90			
	Lig:H22	S503:O	1.74			
	Lig:H19	E410:OE2	1.78			
ZINC71773625	Lig:H27	S501:OG	1.97	D414, E410, Y442, Q183, P180, K415 and T445	-7.625	-70.273
	Lig:H22	G413:O	2.23			
	N444:1HD2	Lig:O1	2.37			
	Lig:H28	G413:O	2.29			
	Lig:H30	E443:OE2	1.78			
	Lig:H31	E410:OE2	1.76			
	G502:H	Lig:O5	1.83			

Conclusion

Housekeeping functionality of ASM is essential to reduce avoid the occurrence of lysosomal storage disorder, Niemann-Pick disease. Conversely, translocation of ASM to plasma membrane by PKCδ phosphorylation, and its subsequent regulation of ceramide level elevation leads AD pathology. Our structural analysis of ASM and PKCδ, and their protein-protein docking and dynamics demonstrate an interface of ASM that binds to PKCδ. Screening of large small molecules against to ASM by molecular docking led us to identify hit molecules, which possess interacting efficacy. The top four compounds, ZINC85551993 (3'-Sialyllactose), ZINC71928291 (neomycin), ZINC85432419 and ZINC71773625 (rapastinel) showed interactions with residues of ASM, which are essential to make ASM-PKCδ. The existing pro-apoptotic, anti-microbial and anti-depressant activities of ZINC85551993 (3'-Sialyllactose), ZINC71928291 (neomycin) and ZINC71773625 (rapastinel), respectively, and the proven apoptotic role of ASM together supports a possibility that these molecules may act as potential allosteric inhibitors of ASM. Taken together, the four lead molecules may developed as allosteric modulators of ASM for the hope of AD therapeutic implications.

Declarations

Funding

Authors are grateful to University Grants Commission, India for their financial support. We would like to thank Department of Biotechnology (DBT), India for providing computational facilities.

Ethics Declarations

The authors declare no competing interests

Availability data and materials

All the data generated during this study is included in the manuscript

Code Availability

Software application

Contributions

Yellamandayya Vadlamudi: Molecular docking, Molecular modelling and molecular dynamics simulation studies, and manuscript writing

Kannan M: PCA analysis

Thirunavukkarasu C: Scientific discussion of study

Suresh Kumar M: Supervision and manuscript review and editing

References

1. (2013) 2013 Alzheimer's disease facts and figures. Alzheimer's Dement. https://doi.org/10.1016/j.jalz.2013.02.003
2. Gaugler J, James B, Johnson T, et al (2016) 2016 Alzheimer's disease facts and figures. Alzheimer's Dement. https://doi.org/10.1016/j.jalz.2016.03.001
3. Brunkhorst R, Vutukuri R, Pfeilschifter W (2014) Fingolimod for the treatment of neurological diseases—state of play and future perspectives3. Front Cell Neurosci 8:1–20. https://doi.org/10.3389/fncel.2014.00283

4. Braak H, Alafuzoff I, Arzberger T, et al (2006) Staging of Alzheimer disease-associated neurofibrillary pathology using paraffin sections and immunocytochemistry. Acta Neuropathol. https://doi.org/10.1007/s00401-006-0127-z
5. Budson AE, Solomon PR (2012) New criteria for Alzheimer disease and mild cognitive impairment: Implications for the practicing clinician. Neurologist
6. Beach TG, Schneider JA, Sue LI, et al (2014) Theoretical impact of florbetapir (18F) amyloid imaging on diagnosis of Alzheimer dementia and detection of preclinical cortical amyloid. J Neuropathol Exp Neurol. https://doi.org/10.1097/NEN.0000000000000114
7. Hampel H, Bürger K, Teipel SJ, et al (2008) Core candidate neurochemical and imaging biomarkers of Alzheimer's disease. Alzheimer's Dement. https://doi.org/10.1016/j.jalz.2007.08.006
8. Shen Y, Wang H, Sun Q, et al (2018) Increased Plasma Beta-Secretase 1 May Predict Conversion to Alzheimer's Disease Dementia in Individuals With Mild Cognitive Impairment. Biol Psychiatry. https://doi.org/10.1016/j.biopsych.2017.02.007
9. Dong H, Li J, Huang L, et al (2015) Serum MicroRNA profiles serve as novel biomarkers for the diagnosis of alzheimer's disease. Dis Markers. https://doi.org/10.1155/2015/625659
10. Howard R, McShane R, Lindesay J, et al (2012) Donepezil and Memantine for Moderate-to-Severe Alzheimer's Disease. N Engl J Med. https://doi.org/10.1056/nejmoa1106668
11. Grossberg GT, Manes F, Allegri RF, et al (2013) The safety, tolerability, and efficacy of once-daily memantine (28 mg): A multinational, randomized, double-blind, placebo-controlled trial in patients with moderate-to-severe alzheimer's disease taking cholinesterase inhibitors. CNS Drugs. https://doi.org/10.1007/s40263-013-0077-7
12. Xing SH, Zhu CX, Zhang R, An L (2014) Huperzine A in the treatment of alzheimer's disease and vascular dementia: A meta-analysis. Evidence-based Complement. Altern. Med.
13. Lee LK, Shahar S, Chin AV, Yusoff NAM (2013) Docosahexaenoic acid-concentrated fish oil supplementation in subjects with mild cognitive impairment (MCI): A 12-month randomised, double-blind, placebo-controlled trial. Psychopharmacology (Berl). https://doi.org/10.1007/s00213-012-2848-0
14. Bo Y, Zhang X, Wang Y, et al (2017) The n-3 polyunsaturated fatty acids supplementation improved the cognitive function in the Chinese elderly with mild cognitive impairment: A double-blind randomized controlled trial. Nutrients. https://doi.org/10.3390/nu9010054
15. Chew H, Solomon VA, Fonteh AN (2020) Involvement of Lipids in Alzheimer's Disease Pathology and Potential Therapies. Front. Physiol.
16. He X, Huang Y, Li B, et al (2010) Deregulation of sphingolipid metabolism in Alzheimer's disease. Neurobiol Aging. https://doi.org/10.1016/j.neurobiolaging.2008.05.010
17. Dinkins MB, Dasgupta S, Wang G, et al (2015) The 5XFAD mouse model of Alzheimer's disease exhibits an age-dependent increase in anti-ceramide IgG and exogenous administration of ceramide further increases anti-ceramide titers and amyloid plaque burden. J Alzheimer's Dis. https://doi.org/10.3233/JAD-150088

18. Fassbender K, Simons M, Bergmann C, et al (2001) Simvastatin strongly reduces levels of Alzheimer's disease β-amyloid peptides Aβ42 and Aβ40 in vitro and in vivo. Proc Natl Acad Sci U S A 98:5856–5861. https://doi.org/10.1073/pnas.081620098
19. Dinkins MB, Dasgupta S, Wang G, et al (2014) Exosome reduction invivo is associated with lower amyloid plaque load in the 5XFAD mouse model of Alzheimer's disease. Neurobiol Aging 35:1792–1800. https://doi.org/10.1016/j.neurobiolaging.2014.02.012
20. Coant N, Sakamoto W, Mao C, Hannun YA (2017) Ceramidases, roles in sphingolipid metabolism and in health and disease. Adv. Biol. Regul.
21. Goi FM, Alonso A (2002) Sphingomyelinases: Enzymology and membrane activity. FEBS Lett.
22. Kornhuber J, Müller CP, Becker KA, et al (2014) The ceramide system as a novel antidepressant target. Trends Pharmacol. Sci.
23. Lee JK, Jin HK, Park MH, et al (2014) Acid sphingomyelinase modulates the autophagic process by controlling lysosomal biogenesis in Alzheimer's disease. J Exp Med. https://doi.org/10.1084/jem.20132451
24. Abe A, Shayman JA (2013) Sphingolipid Catabolism. In: Encyclopedia of Biological Chemistry: Second Edition. Elsevier Inc., pp 287–292
25. Charruyer A, Grazide S, Bezombes C, et al (2005) UV-C light induces raft-associated acid sphingomyelinase and JNK activation and translocation independently on a nuclear signal. J Biol Chem. https://doi.org/10.1074/jbc.M412867200
26. Zeidan YH, Hannun YA (2007) Activation of acid sphingomyelinase by protein kinase Cδ-mediated phosphorylation. J Biol Chem 282:11549–11561. https://doi.org/10.1074/jbc.M609424200
27. Phan TG, Wright PM, Markus R, et al (2002) Salvaging the ischaemic penumbra: More than just reperfusion? Clin. Exp. Pharmacol. Physiol.
28. Bright R, Raval AP, Dembner JM, et al (2004) Protein kinase C δ mediates cerebral reperfusion injury In Vivo. J Neurosci 24:6880–6888. https://doi.org/10.1523/JNEUROSCI.4474-03.2004
29. Dave KR, Bhattacharya SK, Saul I, et al (2011) Activation of protein kinase c delta following cerebral ischemia leads to release of cytochrome c from the mitochondria via bad pathway. PLoS One. https://doi.org/10.1371/journal.pone.0022057
30. Tonda-Turo C, Origlia N, Mattu C, et al (2018) Current Limitations in the Treatment of Parkinson's and Alzheimer's Diseases: State-of-the-Art and Future Perspective of Polymeric Carriers. Curr Med Chem. https://doi.org/10.2174/0929867325666180221125759
31. Chivian D, Baker D (2006) Homology modeling using parametric alignment ensemble generation with consensus and energy-based model selection. Nucleic Acids Res. https://doi.org/10.1093/nar/gkl480
32. Kim DE, Chivian D, Baker D (2004) Protein structure prediction and analysis using the Robetta server. Nucleic Acids Res. https://doi.org/10.1093/nar/gkh468

33. A F (2012) Comparative protein structure modeling of genes and genomes. J Proteomics Bioinform. https://doi.org/10.4172/0974-276x.s1.064
34. Shen M, Sali A (2006) Statistical potential for assessment and prediction of protein structures. Protein Sci. https://doi.org/10.1110/ps.062416606
35. Lüthy R, Bowie JU, Eisenberg D (1992) Assessment of protein models with three-dimensional profiles. Nature. https://doi.org/10.1038/356083a0
36. Vadlamudi Y, Muthu K, Suresh Kumar M (2016) Structural exploration of acid sphingomyelinase at different physiological pH through molecular dynamics and docking studies. RSC Adv 6:74859–74873. https://doi.org/10.1039/c6ra16584b
37. Xiong ZJ, Huang J, Poda G, et al (2016) Structure of Human Acid Sphingomyelinase Reveals the Role of the Saposin Domain in Activating Substrate Hydrolysis. J Mol Biol. https://doi.org/10.1016/j.jmb.2016.06.012
38. Hess B, Kutzner C, Van Der Spoel D (2008) GROMACS 4: Algorithms for Highly Efficient, Load-Balanced, and Scalable Molecular Simulation - Journal of Chemical Theory and Computation (ACS Publications). J Chem …
39. Van Der Spoel D, Lindahl E, Hess B, et al (2005) GROMACS: Fast, flexible, and free. J. Comput. Chem.
40. Collier G, Vellore NA, Latour RA, Stuart SJ (2009) Development of molecular simulation methods to accurately represent protein-surface interactions: Method assessment for the calculation of electrostatic effects. Biointerphases. https://doi.org/10.1116/1.3266417
41. Martoňák R, Laio A, Parrinello M (2003) Predicting Crystal Structures: The Parrinello-Rahman Method Revisited. Phys Rev Lett. https://doi.org/10.1103/PhysRevLett.90.075503
42. Amadei A, Linssen ABM, Berendsen HJC (1993) Essential dynamics of proteins. Proteins Struct Funct Bioinforma. https://doi.org/10.1002/prot.340170408
43. Hess B (2000) Similarities between principal components of protein dynamics and random diffusion. Phys Rev E - Stat Physics, Plasmas, Fluids, Relat Interdiscip Top. https://doi.org/10.1103/PhysRevE.62.8438
44. Maisuradze GG, Leitner DM (2007) Free energy landscape of a biomolecule in dihedral principal component space: Sampling convergence and correspondence between structures and minima. Proteins Struct Funct Genet. https://doi.org/10.1002/prot.21344
45. De Vries SJ, Van Dijk ADJ, Krzeminski M, et al (2007) HADDOCK versus HADDOCK: New features and performance of HADDOCK2.0 on the CAPRI targets. In: Proteins: Structure, Function and Genetics
46. Dominguez C, Boelens R, Bonvin AMJJ (2003) HADDOCK: A protein-protein docking approach based on biochemical or biophysical information. J Am Chem Soc. https://doi.org/10.1021/ja026939x
47. Evgeny K (2010) Crystal contacts as nature's docking solutions. J Comput Chem. https://doi.org/10.1002/jcc.21303
48. Krissinel E, Henrick K (2007) Inference of Macromolecular Assemblies from Crystalline State. J Mol Biol. https://doi.org/10.1016/j.jmb.2007.05.022

49. Fogolari F, Brigo A, Molinari H (2003) Protocol for MM/PBSA molecular dynamics simulations of proteins. Biophys J. https://doi.org/10.1016/S0006-3495(03)74462-2
50. Gohlke H, Case DA (2004) Converging Free Energy Estimates: MM-PB(GB)SA Studies on the Protein-Protein Complex Ras-Raf. J Comput Chem. https://doi.org/10.1002/jcc.10379
51. McGovern MM, Avetisyan R, Sanson BJ, Lidove O (2017) Disease manifestations and burden of illness in patients with acid sphingomyelinase deficiency (ASMD). Orphanet J. Rare Dis.
52. Schuchman EH, Desnick RJ (2017) Types A and B Niemann-Pick disease. Mol. Genet. Metab.
53. Lipiński P, Kuchar L, Zakharova EY, et al (2019) Chronic visceral acid sphingomyelinase deficiency (Niemann-Pick disease type B) in 16 Polish patients: Long-term follow-up. Orphanet J Rare Dis. https://doi.org/10.1186/s13023-019-1029-1
54. Opoka L, Wyrostkiewicz D, Radwan-Rohrenschef P, et al (2020) Combined emphysema and interstitial lung disease as a rare presentation of pulmonary involvement in a patient with chronic visceral acid sphingomyelinase deficiency (Niemann-pick disease type b). Am J Case Rep. https://doi.org/10.12659/AJCR.923394
55. Deodato F, Boenzi S, Taurisano R, et al (2018) The impact of biomarkers analysis in the diagnosis of Niemann-Pick C disease and acid sphingomyelinase deficiency. Clin Chim Acta. https://doi.org/10.1016/j.cca.2018.08.039
56. Sillence DJ (2001) Apoptosis and signalling in acid sphingomyelinase deficient cells. BMC Cell Biol. https://doi.org/10.1186/1471-2121-2-24
57. Albi E, Cataldi S, Ceccarini MR, et al (2019) Gentamicin targets acid sphingomyelinase in cancer: The case of the human gastric cancer NCI-N87 cells. Int J Mol Sci. https://doi.org/10.3390/ijms20184375
58. Donello JE, Banerjee P, Li YX, et al (2018) Positive N-Methyl-D-Aspartate Receptor Modulation by Rapastinel Promotes Rapid and Sustained Antidepressant-Like Effects. Int J Neuropsychopharmacol. https://doi.org/10.1093/ijnp/pyy101

Figures

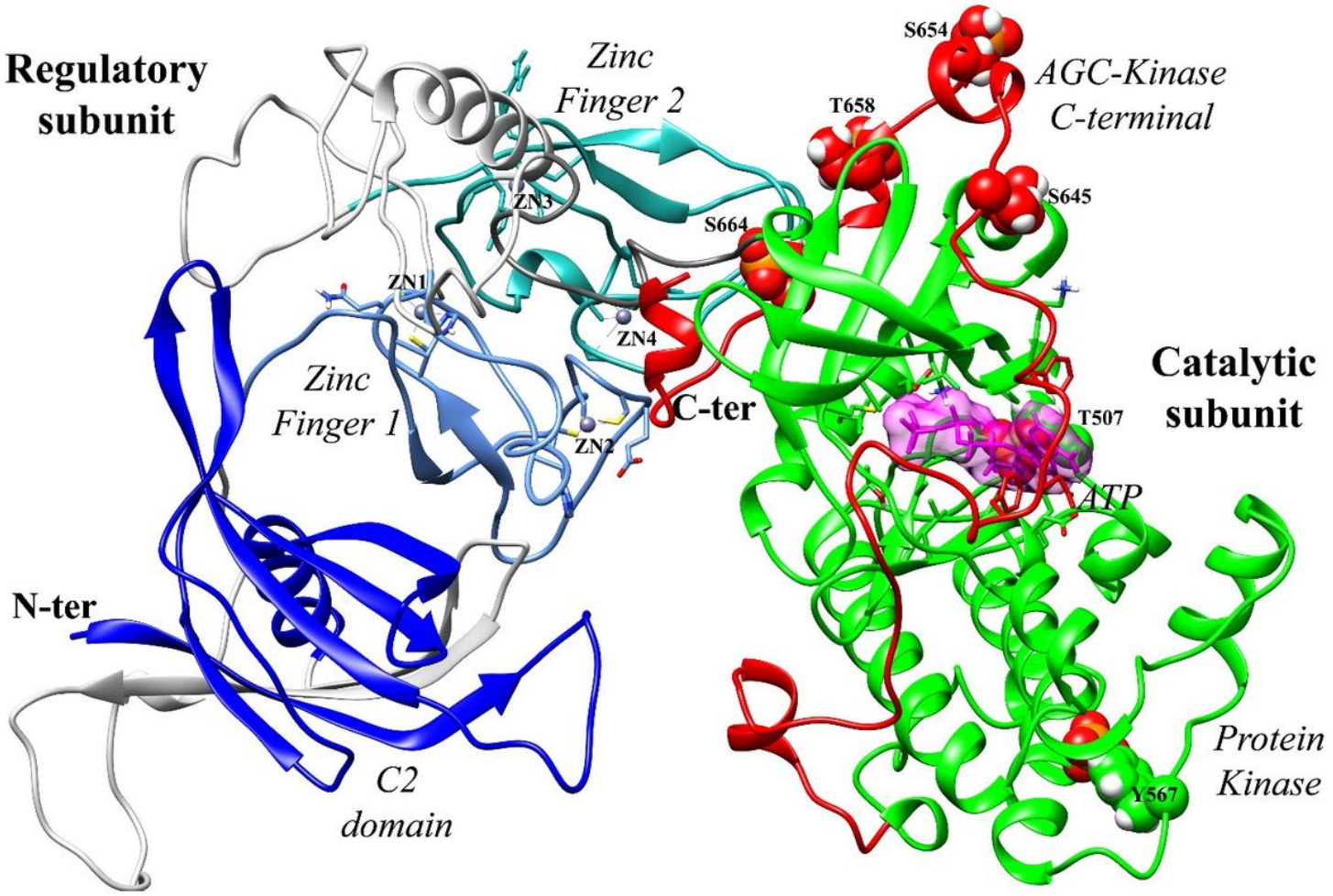

Figure 1

Structure of Protein kinase C δ: The structure contains two subunits namely, regulatory subunit and a catalytic subunit. The regulatory subunit comprises of C2 domain (blue), Zinc finger1 domain (sea blue) and Zinc finger2 domain (cyan). The catalytic domain contains a protein kinase domain (green) and AGC kinase domain (red). ATP (magenta) binds at ATP binding site. The residues that are shown in spherical shape are believed to be involved in auto phosphorylation.

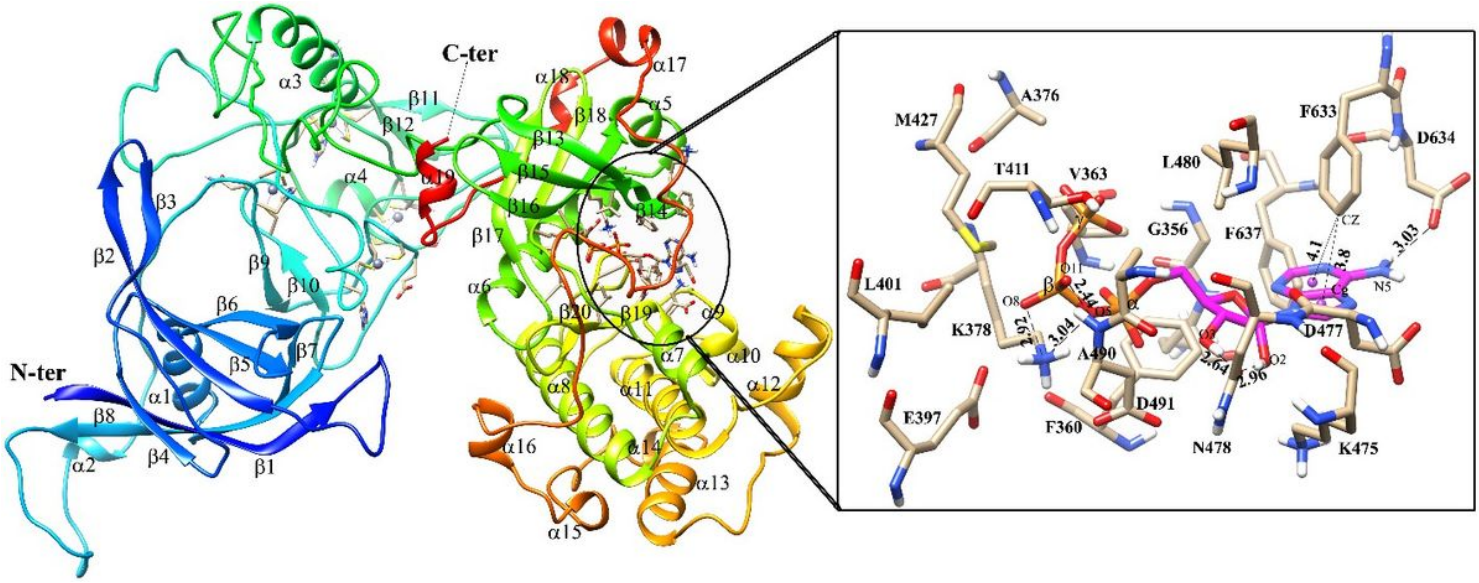

Figure 2

ATP- PKCδ interactions: ATP molecule binds at ATP binding site of PKCδ (circle). The zoomed image shows the ATP and its interacting residues.

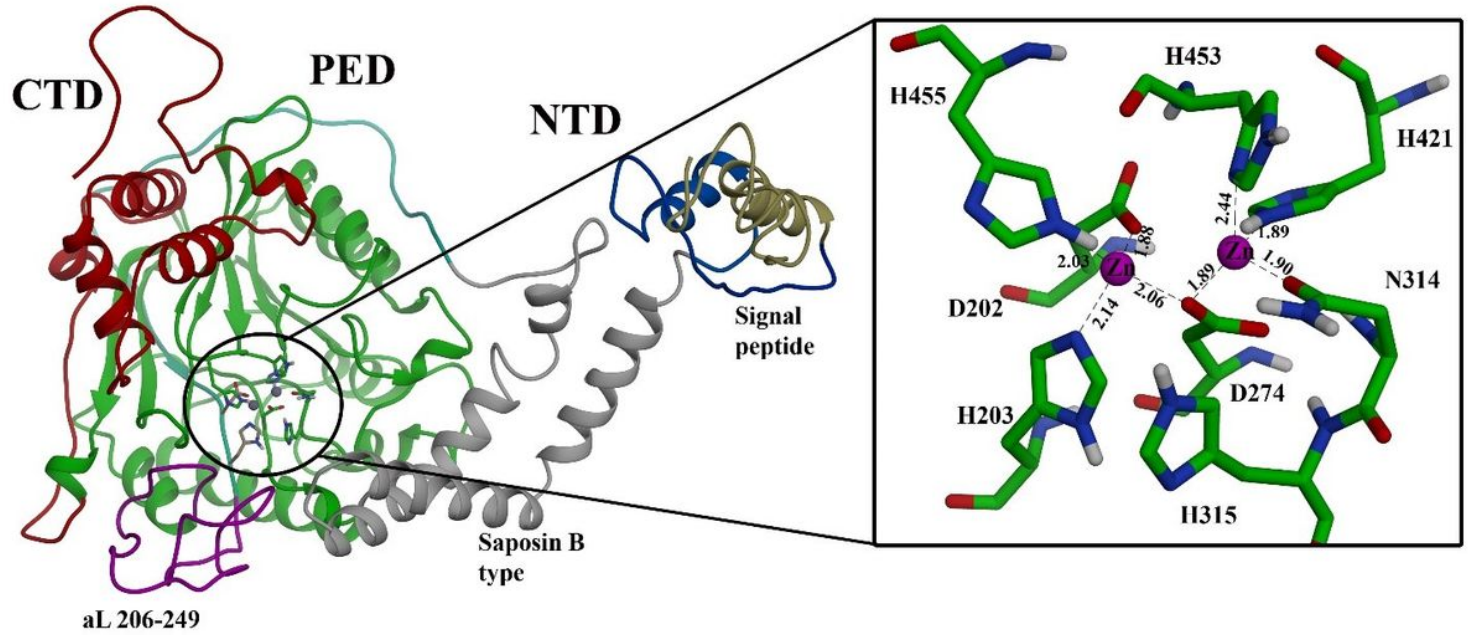

Figure 3

Structure of ASM: The full length ASM three dimentional structure contains N-terminal domain (NTD: 1–184), phosphoesterase domain (PED: 185–524 green) and C-terminal domain (CTD: 525–625 red). NTD holds two sub domain called signal peptide (1–40 sandy brown) and saposin B type domain (81–165 ash). The loop region which is not solved is shown in magenta colour. The zoomed image shows the co-ordinate interaction of two zinc ions with the catalytic cavity of PED domain. The co-ordination interactions are shown in dashed line and Zn2+ in magenta.

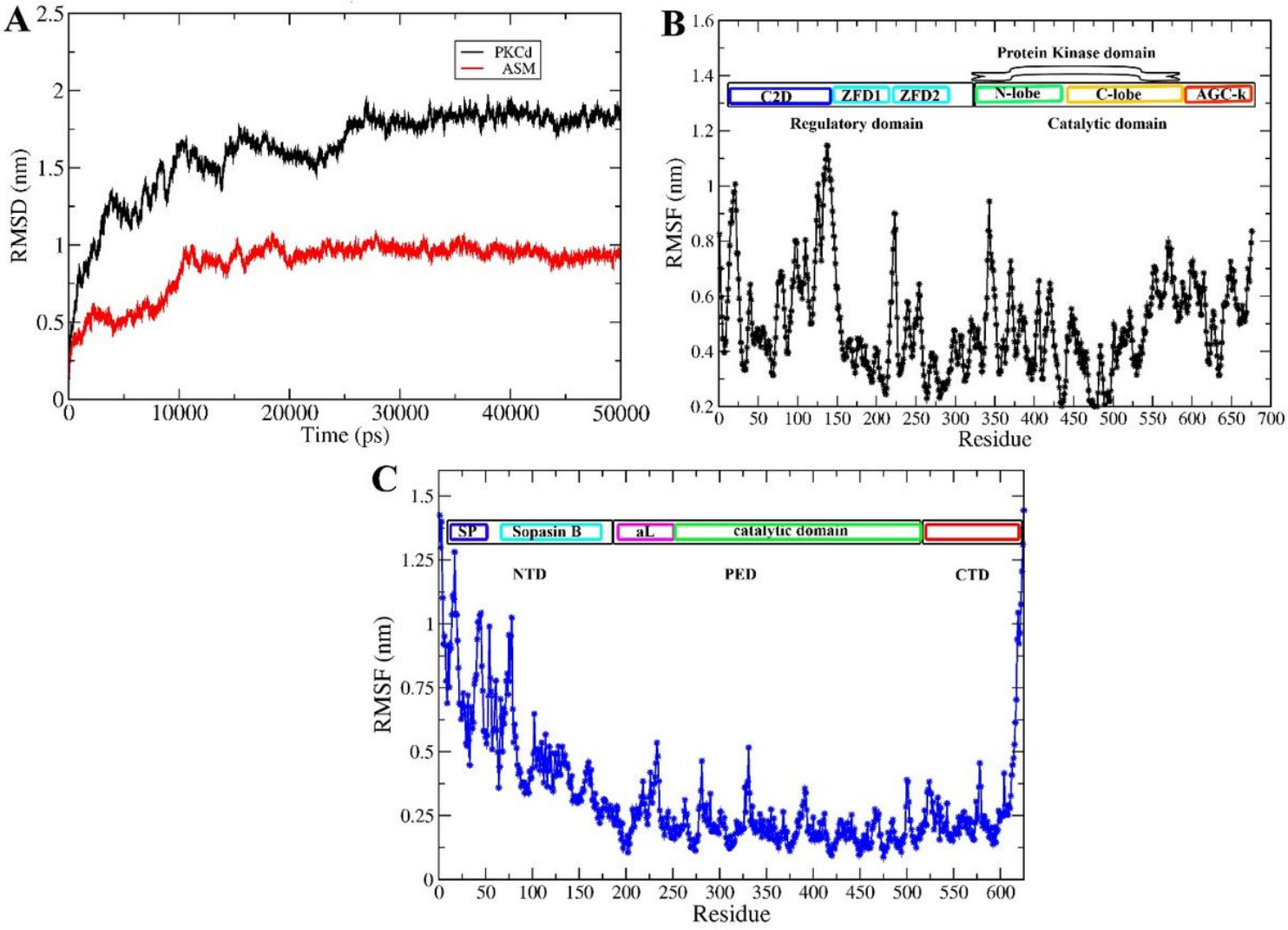

Figure 4

Structural stability analyses of PKCδ and ASM: A) RMSD profile describes the equilibration states and structural stability of PKCδ (black) and ASM (red). B) RMS fluctuations graph of PKCδ and C) RMS fluctuation graph of ASM.

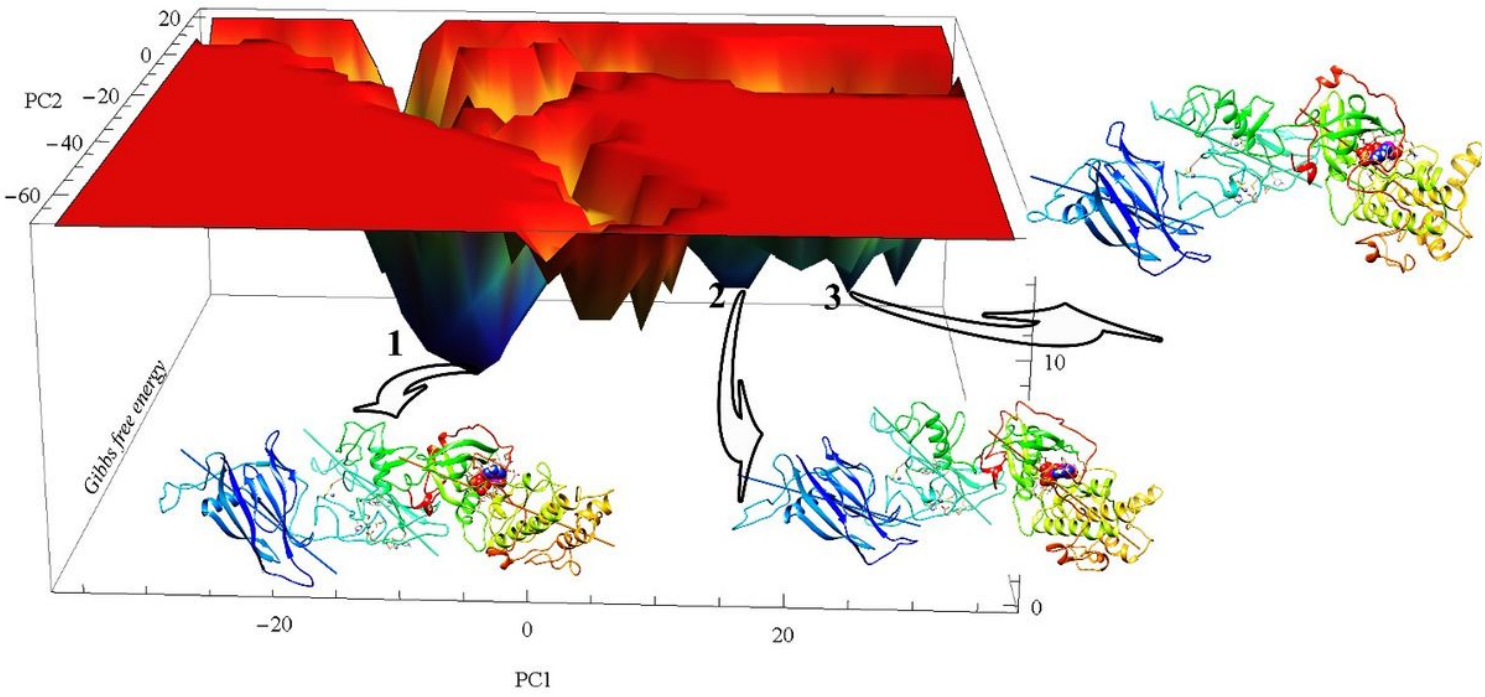

Figure 5

Free energy landscape of PKCδ: FEL map was generated based on first two principle components whose cosine content value is less than 0.2. It shows three different clusters named as 1 to 3 based on the population size. Three representative structure extracted from each cluster were shown.

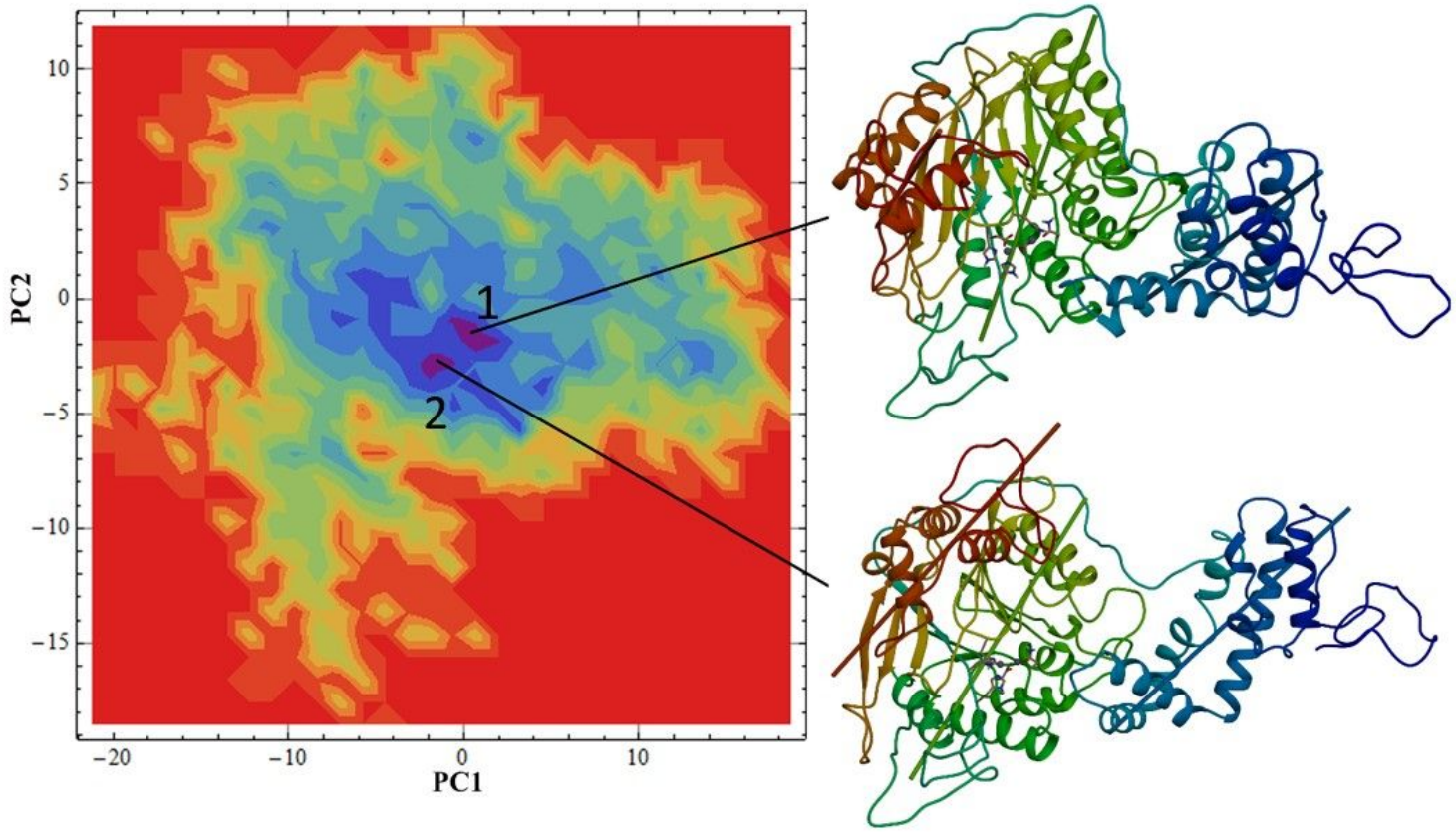

Figure 6

Free Energy Landscape of ASM: The map was derived based on the first two principle components whose cosine content values are lesser than 0.2. Two representative structures were derived from each cluster to understand domain movements.

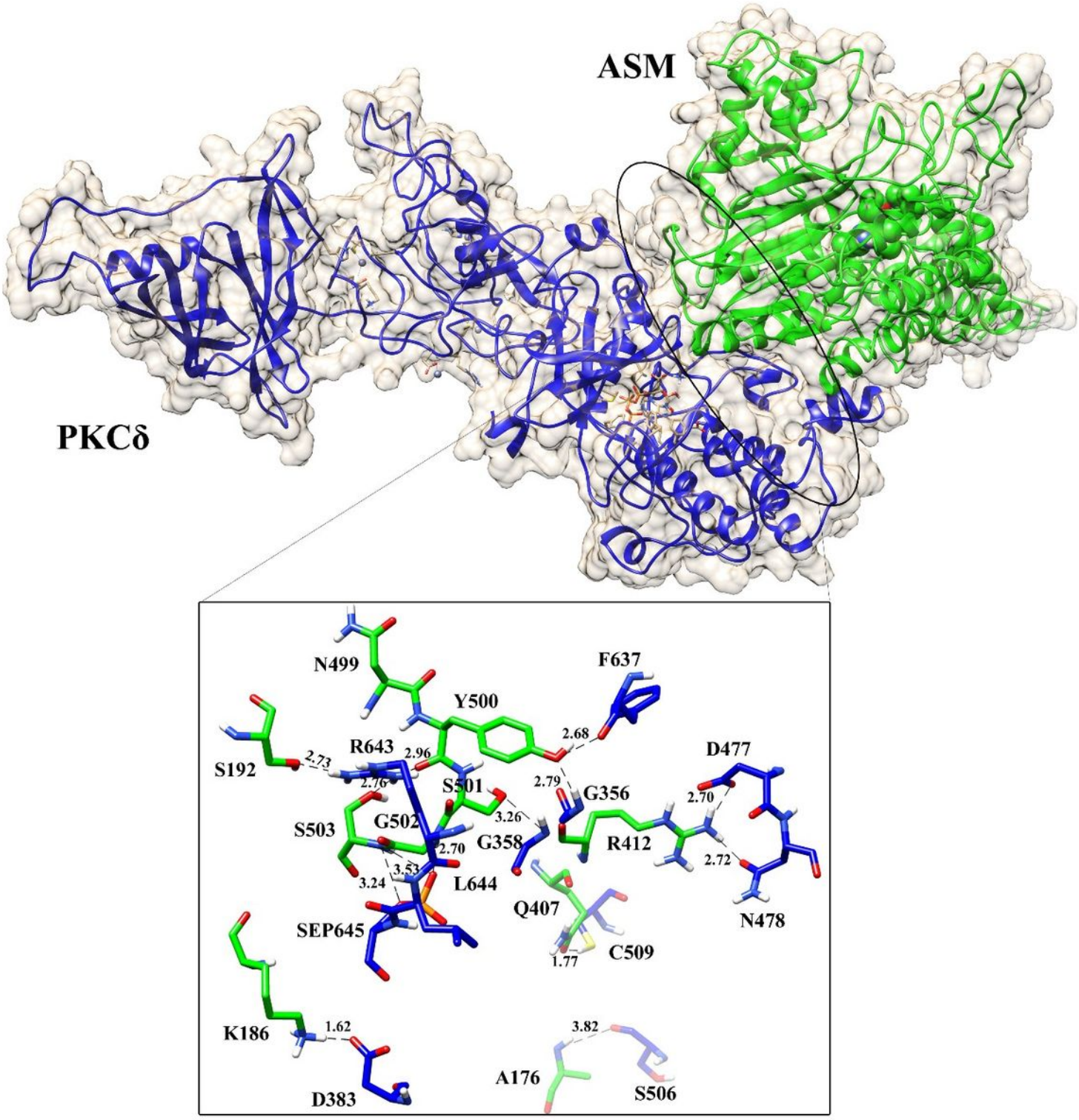

Figure 7

The bio-molecular complex of ASM with PKCδ: The best free energy representative structure of ASM (green) and PKCδ (blue) were docked and the complex is displayed here along with the interacting

residues of ASM and PKCδ.

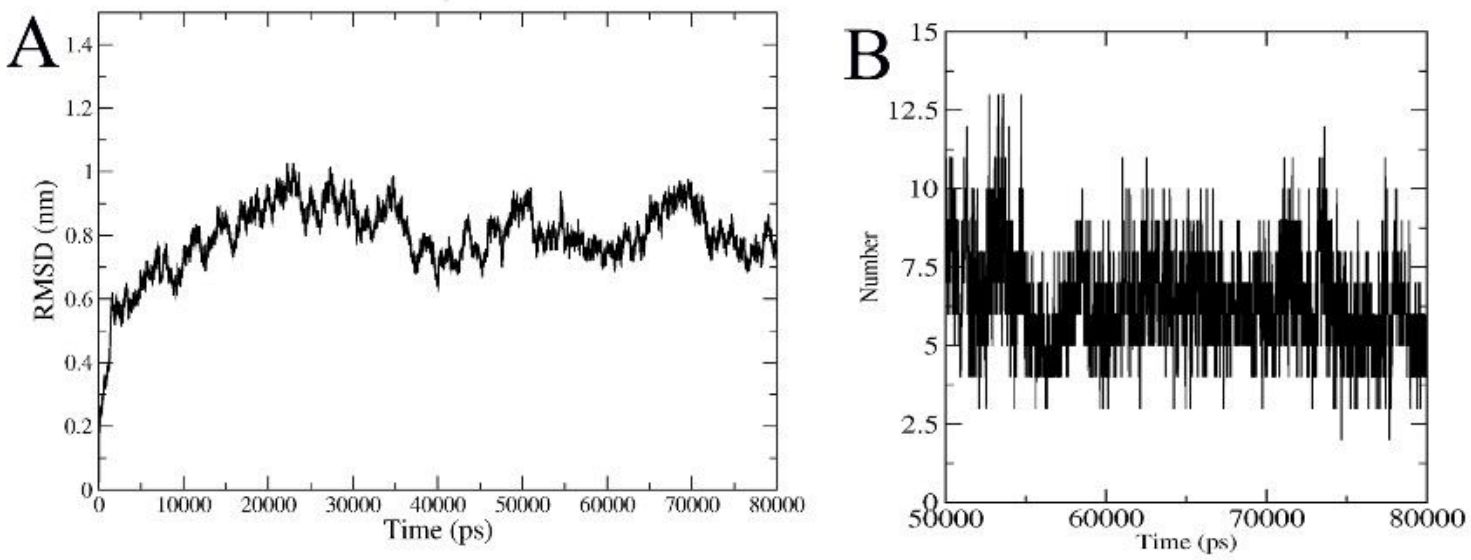

Figure 8

Structural stability analyses of PKCδ-ASM: A) The backbone RMSD of complex structure for 80 ns MD run. B) Hydrogen bond formation for equilibration region of MDS.

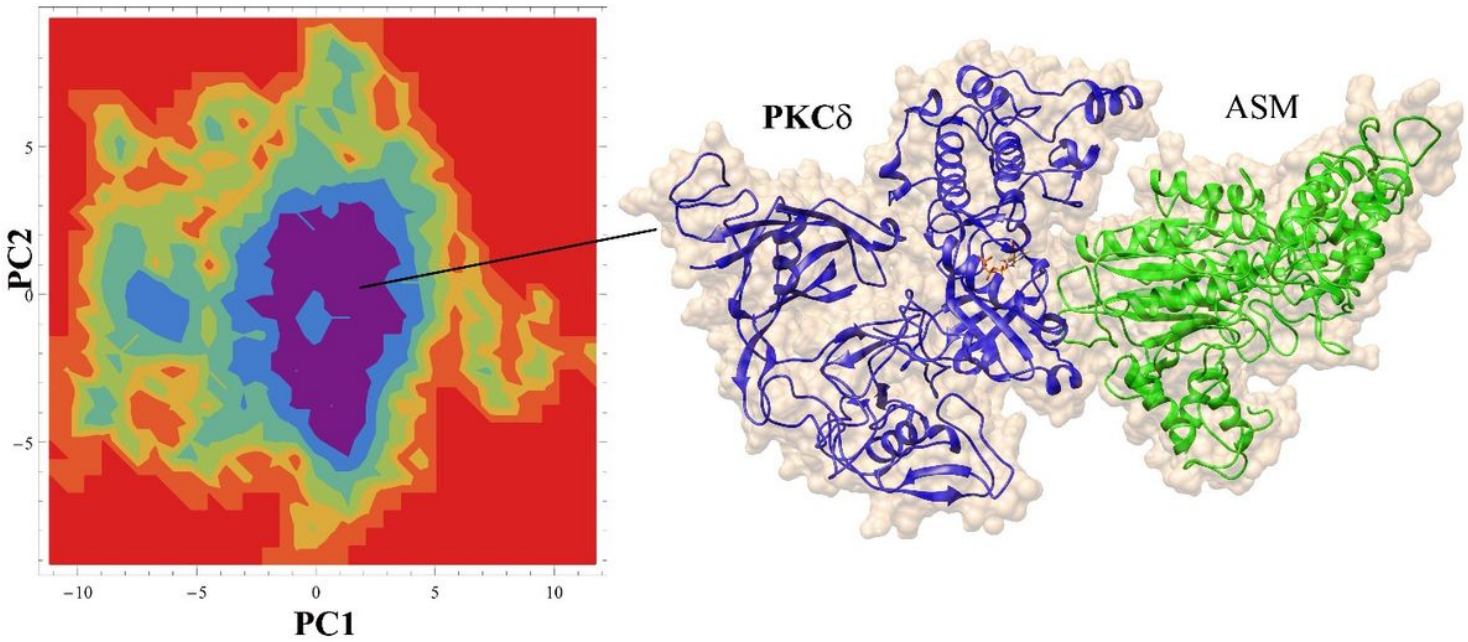

Figure 9

Free energy landscape of complex structure: The most populated cluster was generated and the representative structure conformation was shown.

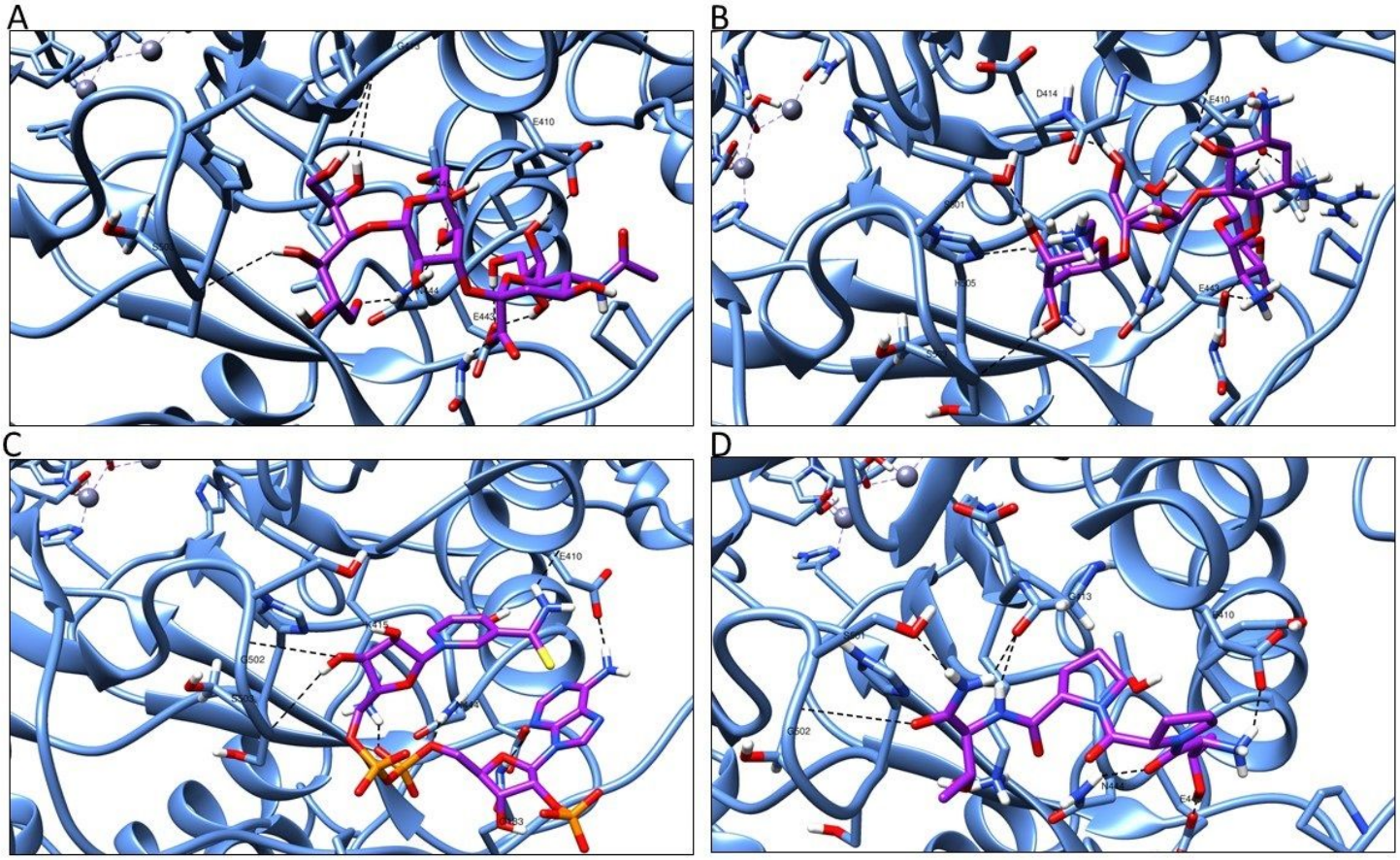

Figure 10

Interaction modes of the best four ligands with allosteric site of ASM: A) ZINC85551993, B) ZINC71928291, C) ZINC85432419, and D) ZINC71773625. Hydrogen bonding shown as black dashed lines.